Surface & Coatings Technology 499 (2025) 131897

Contents lists available at ScienceDirect

Surface & Coatings Technology

journal homepage: www.elsevier.com/locate/surfcoat

Deposition of amorphous SiC coatings by RF sputtering and properties optimization for multifunctional barrier applications in the breeding blanket of nuclear fusion reactors

G. de la Cuerda-Velázquez [a,b,*], E. Carella [c], M. Monclús [d], Y. Mendez-González [a,b], F.J. Sánchez [c], R. Gonzalez-Arrabal [a,b]

[a] Instituto de Fusión Nuclear "Guillermo Velarde", ETSI de Industriales, Universidad Politécnica de Madrid, C/José Gutierrez Abascal, 2, E-28006, Madrid, Spain.
[b] Departamento de Ingeniería Energética, ETSI de Industriales, Universidad Politécnica de Madrid, C/José Gutierrez Abascal, 2, E-28006, Madrid, Spain
[c] National Fusion Laboratory, CIEMAT, Avda. Complutense 40, 28040, Madrid, Spain
[d] IMDEA Materials Institute, c/Eric Kandel 2, Getafe,28906 Madrid, Spain

A B S T R A C T

The development of multifunctional coatings that simultaneously prevent Tritium (T) leaks and Li corrosion of the structural steel is necessary to ensure safe operation of breeding blankets (BBs) that use liquid metals, such as the Water-Cooled Lithium Lead (WCLL) design in nuclear fusion reactors. In this work, we present the development of amorphous Silicon Carbide (a-SiC) coatings deposited by Radio-Frequency (RF) magnetron sputtering as a potential candidate for this application. We characterize the morphology, elemental composition, density, microstructure, hardness and adhesion to the substrate of the coatings as a function of deposition parameters (Ar mass flow rate and bias voltage) and of the bonding material. We observe that low Ar mass flow rates (40 sccm), low bias voltages (-30 V) and Cr bonding lead to amorphous coatings with homogeneous and compact morphology, a high density of 3.15 g/cm^3, and quite good adhesion (critical load of 303 mN) to the steel substrate for the aimed purpose. The studied coatings also present a hardness of 30 GPa and a reduced elastic modulus of 246 GPa. Such combination of properties makes a-SiC coatings a promising candidate to act as a multifunctional barrier in the breeding blanket of nuclear fusion reactors operating both in the inertial and magnetic confinement approaches.

1. Introduction

Nuclear fusion power plants will need to be Tritium (T) self-sufficient since there is no natural source of T that can satisfy their demand beyond the International Experimental Thermonuclear Reactor (ITER). The production of T, together with heat extraction and shielding of other components is one of the main requirements for the breeding blanket (BB). There, T is produced by neutron-induced transmutation reaction of Lithium (Li). A neutron multiplier material such as Beryllium (Be) or Lead (Pb) is also needed to ensure T self-sufficiency (or even surplus) [1]. With these base materials in mind, several BB concepts have been developed, mainly based on solid Li ceramics (such as the helium cooled pebbles bed, HCPB) or liquid eutectic PbLi (such as the water cooled lithium lead, WCLL) [2]. Both designs use a reduced activation ferritic-martesitic (RAFM) such as EUROFER as their structural material due to radiological and technological concerns.

However, not only the production of T is important, but also the control of its inventory, since it has to be enough for self-operation but limited due to safety concerns. Optimal Tritium Breeding Ratio (TBR) values have been reported to be between 1.05 and 1.15 [3]. The control of the T inventory requires to avoid its permeation through the structural steel, since the T leaks would cause a reduction in the recovered T, water activation in those BB concepts that use it as a coolant, and steel embrittlement. These facts are very undesirable from the safety and operational point of view.

Furthermore, BB designs that use a liquid metal (mainly, PbLi) as breeder material face another important issue: the degradation of the structural steel due to a collection of phenomena known as liquid metal embrittlement (LME). LME includes cracking at the interface, diffusion through grain boundaries resulting in decohesion, and various corrosion-type processes such as dealloying [4]. In the case of RAFM steels (such as EUROFER, the European choice for DEMO), one of the most important degradation mechanisms is the dissolution of Cr into the PbLi [5]. Therefore, LME must be prevented in order to ensure the structural integrity of the BB.

One way to simultaneously prevent T leaks and LME is to cover the steel with a multifunctional coating (MFC), which must act simultaneously as a T permeation and Li corrosion barrier while withstanding

* Corresponding author at: Instituto de Fusión Nuclear "Guillermo Velarde", ETSI de Industriales, Universidad Politécnica de Madrid, Madrid, Spain.
E-mail address: g.delacuerda@upm.es (G. de la Cuerda-Velázquez).

https://doi.org/10.1016/j.surfcoat.2025.131897
Received 21 October 2024; Received in revised form 27 January 2025; Accepted 7 February 2025
Available online 10 February 2025

the intense thermal stresses and neutron and gamma irradiation present in the BB. The best candidates for this task are amorphous ceramic coatings: in some cases, they present a dense, compact and homogeneous morphology with no grain boundaries that are ideal to stop both T permeation and LME. In particular, amorphous alumina (Al_2O_3) coatings have been reported to exhibit very high permeation reduction factor (PRF) values [6], while also preserving their morphological integrity after PbLi exposure [7]. However, Li has been shown to penetrate along the whole thickness of these coatings, accumulating close to the coating surface and in the coating/substrate interface [8]. Under real operation conditions (neutron irradiation), this Li is expected to transmute into He and T which could have important drawbacks in the coating performance [9].

This makes the development of alternative MFC materials necessary. In this regard, C-based ceramics are promising candidates due to their low reactivity with Li. In particular, SiC is a very attractive material due to its high thermal stress resistance and low activation among other properties [10,11]. Amorphous SiC (a-SiC) coatings have already been proposed for different BB applications [12,13], and it has been proven to be a great permeation barrier while withstanding simultaneous e- irradiation and thermal cycling [14].

In this work, we focus on the development of a-SiC coatings deposited by radio-frequency (RF) magnetron sputtering. It is worth mentioning that while SiC coatings can also be deposited by other techniques (such as chemical vapor deposition, CVD (thermal-, laser-, halide laser-, hot or warm wall- and halide laser-) [15,16], and pulsed laser deposition, PLD [17]); this physical vapor deposition (PVD) technique presents some key advantages: (i) possibility of tuning the coating properties as desired by adjusting the deposition parameters, (ii) environmentally friendly, (iii) industry-ready technology with easy scalability, (iv) low cost after initial investment and (v) capable of coating complex surfaces [18].

In this work, we study the influence of the deposition parameters (Ar mass flow rate, Φ_{Ar} and bias voltage, V_{bias}) as well as that of the bonding material (Ti, Cr) on the most relevant properties of a-SiC for its application as an MFC: morphology, elemental composition, density, microstructure and mechanical properties; as well as its adhesion to the EUROFER-II substrate. To the best of our knowledge, this is the first time that the density and adhesion of a-SiC coatings to the EUROFER-II substrate have been reported as a function of Φ_{Ar}, V_{bias}, and bonding material, which are key parameters to be considered for the development of suitable MFCs. The final objective is to set the optimal conditions to obtain dense and homogeneous a-SiC coatings with good adhesion to the substrate, ensuring its quality before testing its performance as an MFC.

2. Materials and methods

2.1. Deposition procedure

SiC coatings were deposited both on mirror-polished single-crystalline (100) Si, and polished EUROFER-II steel substrates. Si substrates were used for the morphological, elemental composition, and density studies; while EUROFER-II substrates were used for the microstructural, mechanical and adhesion to the substrate tests. It is worth mentioning that no significant dependence of the coating morphology and microstructure on the substrate was found.

EUROFER-II polishing was performed by sanding down with #500, #800, #1200 and #2400 SiC sandpapers and by sequential mechanical polishing on napless synthetic clothes with colloidal suspensions of varying particle sizes (diamond particles of 6 and 3 μm, and SiO_2 particles of 0.25 μm). Cleaning of the substrates before deposition was performed with ultrasonic washing in alkaline detergents, rinsing with de-ionized water, cleaning with isopropanol and air-drying. After that, they were introduced in the deposition chamber and underwent a plasma etching process in Ar atmosphere. The etching time was 30 min, the DC-pulsed voltage was 400 V, the frequency was 250 kHz, the power was 100 W and the Ar pressure was 8.2×10^{-3} mbar (Φ_{Ar} of 137 sccm) for all samples.

The deposition setup consists of a high vacuum chamber ($P_0 < 7 \times 10^{-6}$ mbar) equipped with two rectangular 20 cm × 7.5 cm magnetrons designed and manufactured by Nano4Energy SL [19]. First, a pure metal bonding layer with a thickness in the nanometer range was deposited by DC magnetron sputtering on the bare EUROFER-II before the deposition of the SiC coating, to improve the adhesion and to mitigate the coefficient of thermal expansion (CTE) mismatch problem [20]. Two different metals were selected: Ti and Cr. Both were deposited at 100 W, from pure (99.95 %) rectangular (20 × 7.5 cm) commercial targets at the same Φ_{Ar} as the corresponding coating. Directly after that and in the same deposition chamber, SiC was deposited by RF sputtering from a nominal SiC (99.95 %) commercial target in the presence of Ar atmosphere (99.9999 % purity) at a plasma power of 300 W. Both depositions took place at a normal incidence angle and at room temperature. In both cases, the target-substrate distance was 12.5 cm.

In order to study the influence of the deposition parameters on the sample properties two series of SiC coatings were deposited. In the first one the Φ_{Ar} was varied from 10 to 170 sccm (corresponding to Ar working pressure from 2×10^{-3} to 1×10^{-2} mbar). Once the Φ_{Ar} range that leads to compact dense and homogeneous coatings was found, its value was fixed at 40 sccm, and a second series was deposited to study the influence of applying a V_{bias}. For that purpose, diverse V_{bias} (-30 V, -60 V and -100 V) were applied to the substrate during the deposition of SiC. Finally, after finding the optimal V_{bias}, a sample using Cr as bonding layer instead of Ti was deposited to study the bonding material influence on the coating's properties. A summary of the fabricated samples together with their deposition conditions is listed in Table 1.

2.2. Elemental, Morphological, and microstructural characterization

The coating morphology and thickness were characterized by Scanning Electron Microscope (SEM) imaging, using a Carl Zeiss Auriga Compact FESEM microscope equipped with Bruker X Flash EDS detector.

The elemental composition was characterized by elastic backscattering spectrometry (EBS) in the standard line of the Cockcroft-Walton (CW) particle accelerator located at *Centro de Micro-Análisis de Materiales – Universidad Autónoma de Madrid* (CMAM-UAM) [21]. Measurements were carried out using a $^4He^+$ beam at 4 MeV. The backscattered ions were detected by a standard solid-state Si-barrier detector placed at 170.5° from the beam direction. The chosen experimental conditions lead to non-Rutherford cross section for C as reported by Leavitt et al., allowing for precise quantification of this element [22]. They also lead to a non-Rutherford cross section for Si, as reported by Cheng et al. [23], that presents a resonance at high energy (~2 MeV product energy). This resonance does not overlap with the C signal and therefore does not reduce the accuracy of the C measurement. The ion beam current was set to ~18 nA, and the beam spot was 1.5 mm in diameter. Each sample was measured until a charge of 15 μC was reached.

The microstructure was characterized by grazing-incident angle

Table 1
Summary of deposition conditions for reported SiC coatings.

Sample Code	Φ_{Ar} (sccm)	V_{bias} (V)	Bonding Material
S1–1	10	0	Ti
S1–2	19	0	Ti
S1–3	40	0	Ti
S1–4	59	0	Ti
S1–5	112	0	Ti
S2–1	40	−30	Ti
S2–2	40	−60	Ti
S2–3	40	−100	Ti
S3–1	40	−30	Cr

(0.5°) X-ray diffraction (GI-XRD), using a Panalytical X-PERT PRO diffractometer with a Cu-K_α ($\lambda = 0.15405$ nm) radiation source. The data were collected in the 2θ range from 20 to 90° and in continuous scan mode. The scan-step was 0.02°.

2.3. Mechanical properties characterization

The mechanical properties of the coatings and their adhesion to the EUROFER-II substrate were characterized using a Hysitron TI950 tri-boindenter. For the characterization of the mechanical properties, a Berkovich diamond indenter was used. Five cyclic indents were carried out to adjust the compliance of the system, and then seven simple

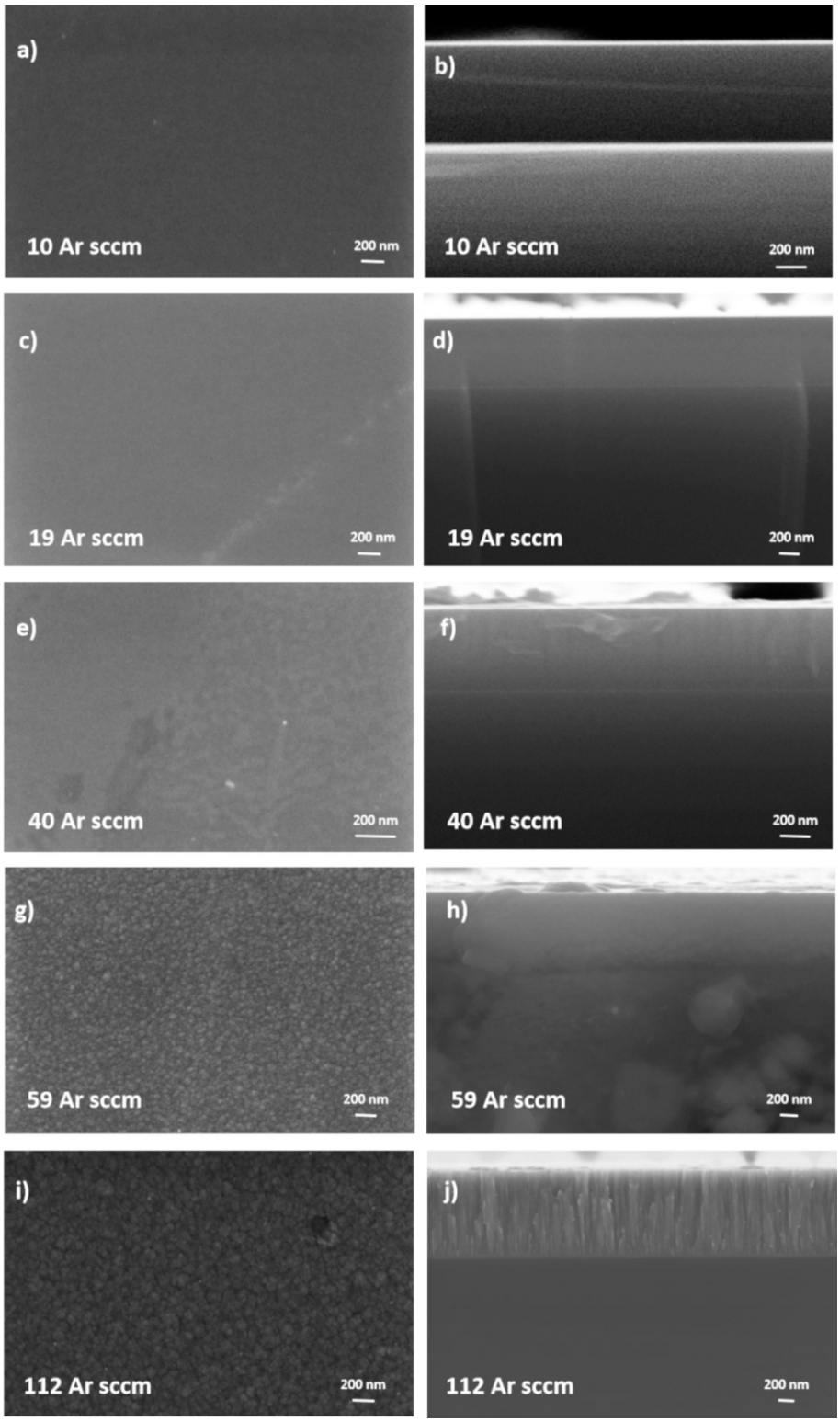

Fig. 1. Top view (left) and cross sectional (right) SEM images for SiC coatings deposited at different Φ_{Ar}.

indents were performed in each sample to obtain reproducible and reliable results. The loading, holding, and unloading times were 5 s, 10 s and 2 s respectively, and the peak load was 10 mN for all measurements. These conditions ensure penetration depths lower than 10 % of the total thickness of the coatings to avoid any influence of the substrate on the measurements. The hardness (H) and the reduced elastic modulus (E_r) were determined from the obtained load-displacement curves using the Oliver & Pharr method [24].

The characterization of the adhesion of the coatings to the EUROFER-II substrate was done by means of nanoscratch. For these measurements, a diamond spheroconical probe with an end radius of 10 μm was used. Progressive load was applied up to a normal force of 350 mN at a loading rate of 11.6 mN/s, while recording lateral force and penetration depth. The scratch length was 400 μm. The critical loads (L_c) were determined by associating sudden changes in the lateral force with the cracking points on the scratches seen by SEM imaging. The test was repeated five times per sample to achieve reliable and accurate results. More information about the adhesion characterization by nanoscratch testing can be found in Ref [25].

3. Results and discussion

3.1. Morphology, thickness and microstructural properties

First, the influence of the Φ_{Ar} on the coating morphology was studied. Top view and cross-sectional SEM images for SiC coatings deposited at different Φ_{Ar} are shown in Fig. 1. The micrographs evidence that the coatings are homogeneous, with no cracks that can hinder performance for the proposed technological application. Cross sectional images show that all coatings have a sharp substrate interface in which no signs of delamination are observed. This is the first indication that the coatings are well adhered to the substrate. The SEM mircographs also show that the coating morphology strongly depends on Φ_{Ar}. At $\Phi_{Ar} \leq 60$ sccm, the coatings are compact whereas at $\Phi_{Ar} > 60$ sccm the coatings exhibit a columnar-like structure with nanocolumns that grow perpendicular to the substrate, having a diameter in the nanometer range that visibly increases with rising Φ_{Ar}. No voids are observed between the nanocolumns within the SEM resolution limit (Fig. 1 – g-j).

In agreement with the Thornton's morphology diagram [26,27], these results evidence that the Φ_{Ar} has a strong influence on the sample morphology. The morphologies observed in the two different Φ_{Ar} regimes are mainly related to the number of collisions that the sputtered atoms suffer with the working gas. In the low Φ_{Ar} regime ($\Phi_{Ar} < 60$ sccm), the number of collisions is low, so sputtered atoms arrive with large momentum, high kinetic energy and low incident angles which lead to compact morphology. The opposite is true in the high Φ_{Ar} regime ($\Phi_{Ar} \geq 60$ sccm), resulting in columnar morphology.

Both of these morphologies have already been reported by other authors for SiC coatings deposited by sputtering (homogeneous in [12,14,28], columnar in [29,30]). In fact, Liu et al. [31] reported the same behavior as the one shown in Fig. 1. However, the Φ_{Ar} at which the transition occurs varies from author to author. This indicates that Φ_{Ar} is not the only parameter influencing this phenomenon: some others such as sputtering power and target-substrate distance may also play a role.

Once the Φ_{Ar} which leads to compact and homogeneous coatings is found, the next step is to study the influence of applying a V_{bias} on the coating morphology. The aim is to further increase the coating density by enhancing the peening effect and the adatom mobility during the coating growth [32]. Fig. 2 shows cross-sectional SEM images for coatings deposited at a constant Φ_{Ar} of 40 sccm (4.9×10^{-3} mbar) and at different V_{bias}. In view of industrial applications, the selection of the Φ_{Ar} was done to have the highest deposition rate (5.3 nm/min) that leads to compact coatings.

In agreement with previous publications [31], no visible differences are observed in the coating morphology for any of the selected V_{bias}. The features seen in Figs. 2a) and c) are produced during the cleaving process and do not correspond to any morphological change. Therefore, we can conclude that, for the selected Φ_{Ar} (40 sccm), the V_{bias} has no influence on the sample morphology. All the coatings, regardless of the applied V_{bias}, are compact.

However, applying a bias changes the coating thickness. It slightly increases for the coating deposited at -30 V V_{bias} (from 1.3 μm to 1.4 μm, reaching a deposition rate of 5.9 nm/min) and decreases for coatings deposited at $V_{bias} > 60$ V (from 1.3 μm to 1.2 μm at −100 V). This

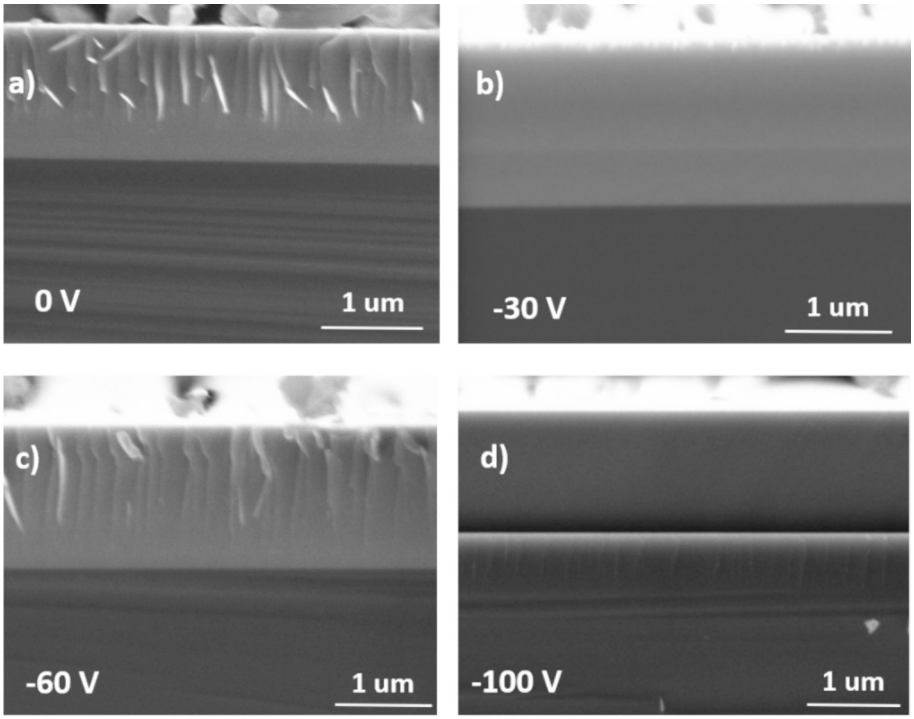

Fig. 2. Cross section images for SiC coatings deposited at a Φ_{Ar} of 40 sccm and different V_{bias}: without biasing (a), −30 V (b), −60 V (c) and -100 V (d).

indicates that at low V_{bias} there is an enhanced energetic ion bombardment that increases the deposition rate [32]. On the other hand, at high V_{bias}, the kinetic energy of the ions is sufficiently high to promote self-sputtering of the coating surface [33]. The latter decreases the coating thickness and compactness, which is not desirable.

The influence of the bonding material on the coating's morphology is also studied. No differences are observed on the morphology of the coating when changing the bonding material from Ti to Cr (not shown).

The normalized GI-XRD patterns for compact SiC coatings deposited on EUROFER-II at different Φ_{Ar} and V_{bias} are shown in Fig. 3-a and b, respectively. Coatings with columnar morphology ($\Phi_{Ar} > 60$ sccm) have been excluded from the analysis, since they do not fulfill the requirements described for MFCs [8]. These samples are not as compact as the ones deposited at $\Phi_{Ar} < 60$ sccm and exhibit a lower density, as further described in section 3.2.

The only sharp peak observed in all spectra is located at $\theta_1 = 45°$ which matches the (100) α-Fe pattern corresponding to the EUROFER substrate. The spectra for the coating deposited at a $V_{bias} = -100$ V exhibits a small peak at $\theta_2 = 65°$ corresponding to the same α-Fe phase (COD ID: 96–900-6602 for both peaks). The variation in peak intensity in Fig. 3-b is caused by the varying thickness of the coatings, which presents its highest value for the −30 V sample.

Apart from the peaks related to the substrate, no other sharp diffraction peak is observed for any other coating, regardless of the Φ_{Ar} or bias voltage values, which shows that the coatings are mainly amorphous. However, the presence of a broad and noisy peak located between 30° and 40° for coatings deposited at a V_{bias} of −30 V and − 60 V (Fig. 3-b) could match the typical range for the most intense SiC diffraction peaks, which could indicate the existence of nanocrystalline inclusions. These have already been reported for SiC coatings deposited by vacuum kinetic spraying [34]. Further research using high resolution techniques (such as electron diffraction patterns from transmission electron microscopy and/or synchrotron techniques) is needed to elucidate this point. Nevertheless, it has been demonstrated that this "amorphization" degree is high enough to make the coatings excellent barriers for tritium permeation as stated in a previous publication for similar "amorphous layers" [14].

Finally, changing the bonding material from Ti to Cr did not result in any difference in the obtained GI-XRD spectra (not shown). Therefore, it is concluded that all SiC coatings that present a compact morphology are also amorphous within the resolution limit of GI-XRD.

3.2. Elemental composition

The elemental composition of the coatings was determined by comparing measured and simulated EBS spectra. The commercial computer code SIMNRA was used for the simulations [35]. The spectra were fitted using a 3-layer model: The SiC coating, the Ti bonding layer, and the Si substrate. A representative fitted EBS spectrum is shown in Fig. 4. The "chi-squared" algorithm was used to determine the accuracy of the peak fit, obtaining, in all cases, χ^2_r values lower than 6. The elemental composition of the coatings is constant regardless of the selected Φ_{Ar}, or V_{bias} or bonding layer. All coatings are non-stoichiometric, having excess C (55 ± 1 at. %).

3.3. Density

The average coating density was calculated by combining data from SEM images (thickness) and EBS measurements (composition and areal density) according to eq. 1:

$$\rho(g/cm^3) = \frac{areal\ density\ (at/cm^3)}{thickness\ (cm)} \left(\frac{[C]\cdot M_{at\ C}}{N_{Av}} + \frac{[Si]\cdot M_{at\ Si}}{N_{Av}} \right) (g/at) \qquad (1)$$

Where ρ represents the density, [C] and [Si] the concentration of each element in at. %, $M_{at\ C/Si}$ the atomic masses, and N_{av} the Avogadro's number.

The calculated density values are shown in Fig. 5-a as a function of Φ_{Ar}. Error bars represent the standard deviation in datapoints where more than one sample was measured. For comparison, the maximum (6H-SiC) and minimum (3C-SiC) density values reported for crystalline

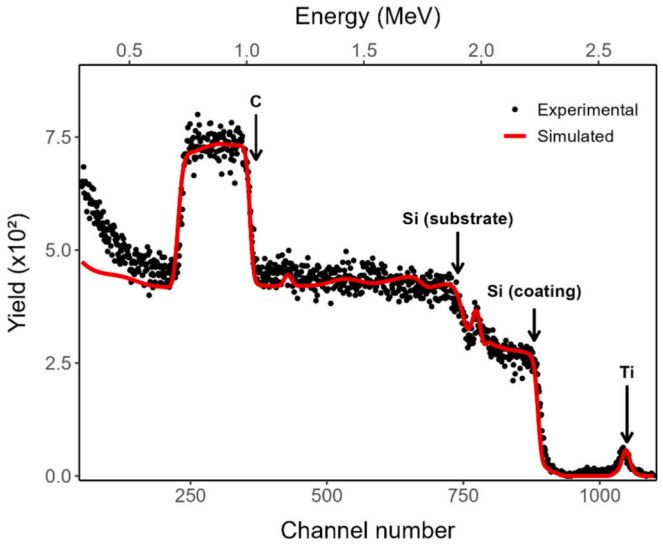

Fig. 4. C and Si content in at. % as a function of Φ_{Ar} during deposition, and miniature of an EBS spectrum of one of the analyzed samples.

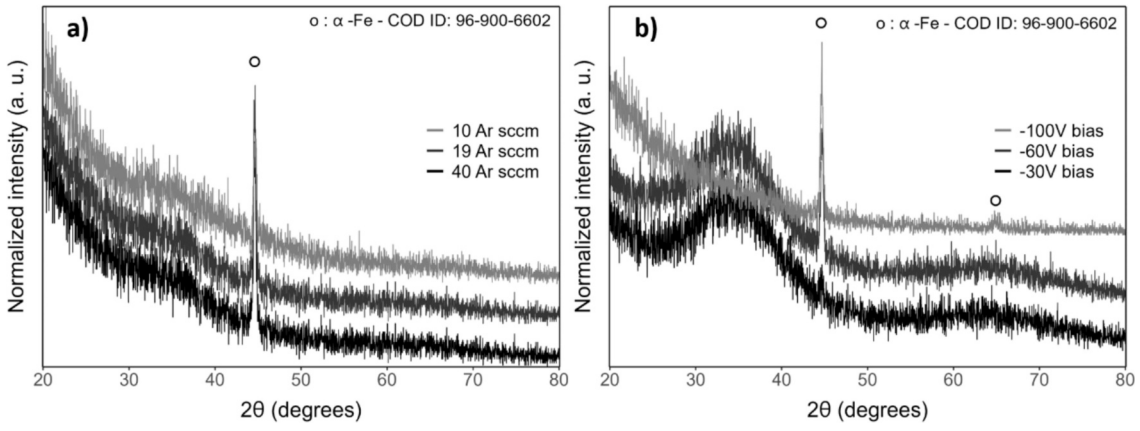

Fig. 3. XRD spectra for as-deposited SiC coatings on EUROFER-II substrates at different ΦAr (a) and at 40 Ar sccm with varying bias voltage (b).

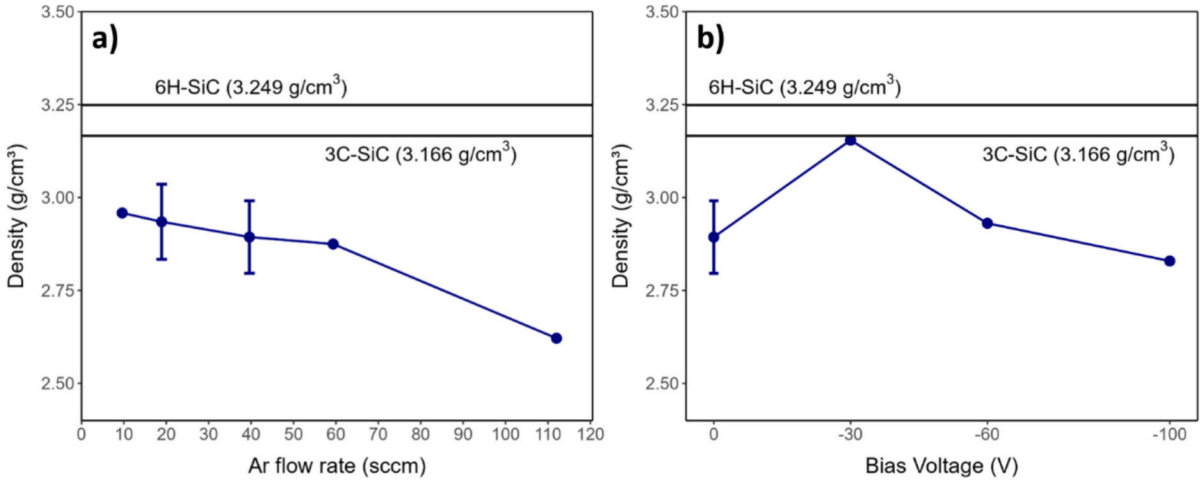

Fig. 5. Calculated density for SiC coatings as a function of (a) Φ_{Ar}.and (b) V_{bias} for coatings deposited at 40 sccm Φ_{Ar}. Maximum (6H-SiC) and minimum (3C-SiC) densities of crystalline SiC phases marked for reference. Values obtained from ref. [11].

SiC are also illustrated [11]. The density calculated for coatings deposited at Φ_{Ar} between 10 and 60 sccm, is constant (2.9 ± 0.1 g/cm^3) within the standard deviation. These values are lower than that reported for the cubic 3C-SiC polytype crystalline phases reported in [11] (3.166 g/cm^3). This can be due to the presence of C excess in the coatings and/or to their amorphous nature. The density of the coating deposited at $\Phi_{Ar} = 112$ sccm strongly decreases. This may be due to their columnar morphology, even when no voids are observed between the columns within the SEM resolution limit. As previously mentioned, the reduced density of columnar SiC coatings will be detrimental to their performance as multifunctional barriers.

Fig. 5-b shows the density of the coatings as a function of the applied V_{bias} for those coatings deposited at a fixed Φ_{Ar} of 40 sccm. Applying a V_{bias} of −30 V, increases the coating density up to 3.15 g/cm^3, which is very close to that reported for the 3C-SiC crystalline phases. At higher V_{bias}, the coating density decreases. At -60 V, the density is in the range of the non-biased sample, while at -100 V the density is in the lower end of the standard deviation range of the non-biased sample. These results show that applying a V_{bias} below the self-sputtering regime leads to densification due to the increase in the kinetic energy of the impinging ions. The decrease in the coatings density observed for higher V_{bias} further indicates that the sputtering of the coating surface has been activated [33].

3.4. Mechanical properties

The hardness (H) and reduced elastic modulus (E_r) of SiC coatings were characterized by nanoindentation. All samples present a H of 30 ± 1 GPa and an E_r of 246 ± 7GPa, with no significant variations. Results reveal that Φ_{Ar}, V_{bias} or bonding material have no influence on H or E_r in the studied ranges.

These coatings present a higher H and lower E_r than crystalline SiC [15], which is expected due to their mainly amorphous microstructure. The H values are also in the range of those reported by other authors working on similar coatings [31,36]. These results contrast somehow with those previously reported in which an influence of these parameters on the mechanical properties of a-SiC is observed [31].

3.5. Adhesion

Fig. 6 shows a detailed SEM image of a typical coating after undergoing a scratch test. The coating shows a brittle response to the increasing normal load, with Hertz cracking and spallation being the most prominent types of cracks [25]. Three critical loads that correspond with different mechanical responses can be defined: (i) Lc_0: Non-elastic response and first surface cracking of the coating. (ii) Lc_1: First, major edge cracking and delamination. Cohesive failure at the interface. (iii) Lc_2: Total coating failure and complete substrate exposure. Lc_1 is the reported critical load, since it is where the first cohesive failure between coating and substrate occurs.

Fig. 7 shows the average critical loads (Lc_1, as defined in Fig. 6) for several a-SiC coatings deposited on EUROFER substrates as a function of Φ_{Ar} (a) and V_{bias} for Φ_{Ar} set at 40 sccm (b). The error bars represent the standard deviation obtained from performing 5 scratches per sample. The data show that Φ_{Ar} has no significant influence on the critical load for the studied range, whereas V_{bias} has. The highest Lc_1 value is obtained for the sample deposited at 40 Ar sccm with -30 V bias, reaching 282.1 ± 12.4 mN. The Lc_1 value for the equivalent non-biased sample is 264.9 ± 4.3 mN. This means that a moderate increase (6.5 %) in adhesion is achieved by applying a small bias. Higher bias values result in a significant drop in adhesion.

The adhesion of the coating to the substrate is also related to the energy of the impinging atoms below the self-sputtering regime. The higher it is, the larger the adhesion. However, this effect is not observed

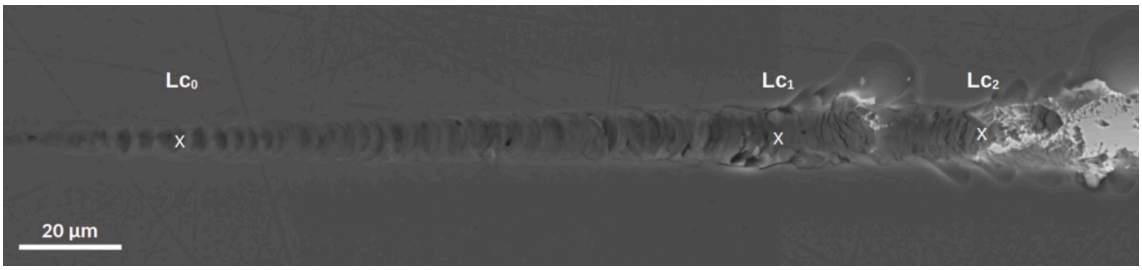

Fig. 6. Detailed SEM image of a scratch performed on an a-SiC coating deposited on a EUROFER-II substrate, with the three critical load points marked for reference.

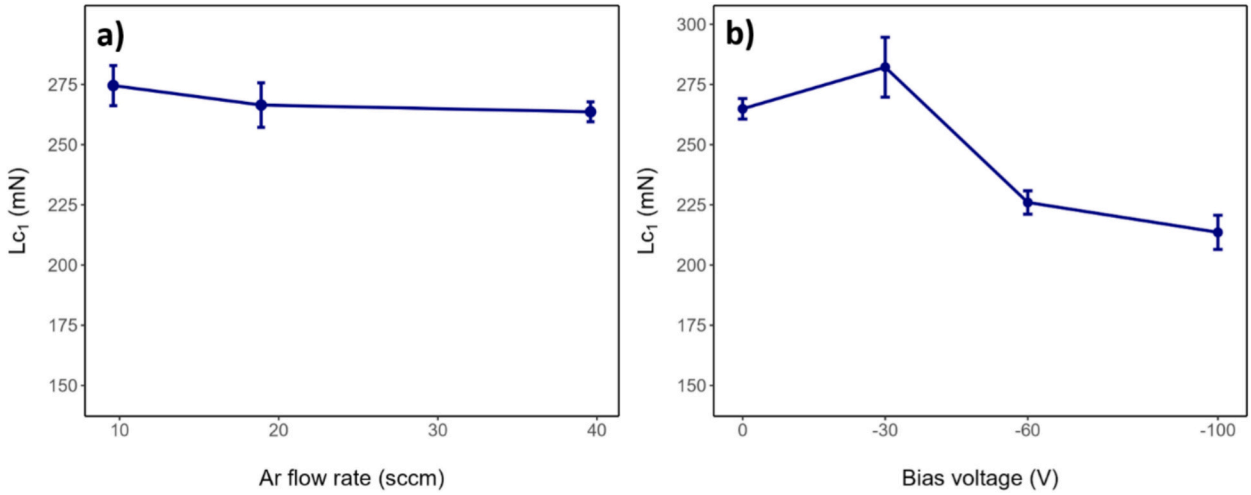

Fig. 7. Average critical load (Lc_1) of a-SiC coatings deposited on EUROFER substrates at varying Φ_{Ar} with no bias voltage (a); and deposited at 40 Ar sccm with varying bias voltage (b).

for the selected Φ_{Ar} values due to the small investigated range. It is noticeable when applying a small V_{bias} (-30 V) due to the increase in kinetic energy of the impinging ions. Higher voltages, on the other hand, are detrimental to the adhesion, due to an excessive increase in the internal stress of the coating. This behavior has also been reported for crystalline TiN and TiN-MoS_x coatings deposited by DC magnetron sputtering [37,38], but other authors have only observed a decrease in adhesion with increasing V_{bias} [39,40]. It is clear that the influence of V_{bias} on adhesion depends on the material and deposition process.

Finally, we compared the effect of using Ti or Cr for the bonding layer on the adhesion of the a-SiC coatings to the EUROFER II substrate. We observe that using Cr as bonding layer instead of Ti does not significantly change fracture mode or the distance between critical loads defined in Fig. 6. However, the use of Cr bonding increases Lc_1 up to 302.8 ± 5.0 mN without notably changing the fracture mode and the distance between critical loads defined in Fig. 6. This represents a 7 % increase when compared to the coating with Ti bonding.

Both Ti a Cr form phases with SiC [41,42], but Cr has greater affinity with the Cr-based EUROFER substrate. Furthermore, first principles calculations show that the work of separation is significantly higher for the crystalline SiC – Cr interface than for the crystalline SiC – Ti one for all studied orientations [43]. Both of these facts can explain the small enhancement in adhesion when using Cr instead of Ti for the bonding layer.

4. Conclusions

In this work, we have successfully optimized the properties of a-SiC coatings deposited by RF sputtering by modifying the Φ_{Ar}, V_{bias} applied to the substrate, and bonding material. The enhanced adatom mobility and increased ion bombardment provided by V_{bias} of -30 V has proven to enhance most properties (density, adhesion, sputtering rate); while higher voltages have been shown to be detrimental due to excessive ion bombardment that triggers self-sputtering of the coating surface. All coatings remain amorphous regardless of the Φ_{Ar}, V_{bias} or bonding material. The configuration that leads to the best a-SiC coating in terms of compactness, density and adhesion is an Φ_{Ar} of 40 sccm with a V_{bias} of -30 V, using a Cr bonding layer. This combination of properties makes this a-SiC coating a promising candidate for its application as an MFC in the BB of nuclear fusion reactors operating both in the inertial and magnetic confinement approaches.

CRediT authorship contribution statement

G. de la Cuerda-Velázquez: Writing – review & editing, Writing – original draft, Visualization, Validation, Investigation, Formal analysis, Data curation, Conceptualization. **E. Carella:** Writing – review & editing, Validation, Supervision, Project administration, Funding acquisition, Conceptualization. **M. Monclús:** Writing – review & editing, Validation, Resources, Investigation, Formal analysis, Data curation. **Y. Mendez-González:** Writing – review & editing, Investigation, Formal analysis, Data curation. **F.J. Sánchez:** Writing – review & editing, Validation, Resources, Investigation, Formal analysis, Data curation. **R. Gonzalez-Arrabal:** Writing – original draft, Validation, Supervision, Resources, Project administration, Funding acquisition, Conceptualization.

Declaration of competing interest

The authors declare that they have no known competing financial interests or personal relationships that could have appeared to influence the work reported in this paper.

Acknowledgments

This research has been funded by the European Union under Grant Agreement N° 101059408 (Tritium Impact and Transfer in Advanced Nuclear reactorS (TITANS) project, funded within HORIZON-EURATOM-2021-NRT-01), by the Convenio Plurianual con la Universidad Politécnica de Madrid en la línea de actuación "Programa de Excelencia para el Profesorado Universitario de la Comunidad de Madrid and by Eurofusion Enable Research CfP-FSD-AWP21-ENR-01 (2021–2025) and by Spanish MICIU through the project EXCORPION (PID2022-141926OA-I00). Views and opinions expressed are, however, those of the author(s) only and do not necessarily reflect those of the European Union. Neither the European Union nor the granting authority can be held responsible for them.

The authors acknowledge the support from the *'Centro de Microanalisis de Materiales (CMAM)—Universidad Autonoma de Madrid'*, for the beam time proposals with codes STD0004/23 and STD0024/23; and its technical staff for their contribution to the operation of the accelerator.

Data availability

Data will be made available on request.

References

[1] F.A. Hernández, P. Pereslavtsev, First principles review of options for tritium breeder and neutron multiplier materials for breeding blankets in fusion reactors, Fusion Engineering and Design 137 (2018) 243–256, https://doi.org/10.1016/j.fusengdes.2018.09.014.

[2] G. Federici, L. Boccaccini, F. Cismondi, M. Gasparotto, Y. Poitevin, I. Ricapito, An overview of the EU breeding blanket design strategy as an integral part of the DEMO design effort, Fusion Engineering and Design 141 (2019) 30–42, https://doi.org/10.1016/j.fusengdes.2019.01.141.

[3] M. Abdou, M. Riva, A. Ying, C. Day, A. Loarte, L.R. Baylor, P. Humrickhouse, T. F. Fuerst, S. Cho, Physics and technology considerations for the deuterium–tritium fuel cycle and conditions for tritium fuel self sufficiency, Nucl. Fusion 61 (2021) 013001, https://doi.org/10.1088/1741-4326/abbf35.

[4] J.E. Norkett, M.D. Dickey, V.M. Miller, A review of liquid metal embrittlement: cracking open the disparate mechanisms, Metall Mater Trans A 52 (2021) 2158–2172, https://doi.org/10.1007/s11661-021-06256-y.

[5] W. Ding, M. Zhang, Z. Jiang, M. Zheng, W. Huang, First principles study on the dissolution corrosion behavior of RAFM steel in the liquid PbLi, J. Nucl. Mater. 563 (2022) 153634, https://doi.org/10.1016/j.jnucmat.2022.153634.

[6] D. Iadicicco, S. Bassini, M. Vanazzi, P. Muñoz, A. Moroño, T. Hernandez, I. García-Cortés, F.J. Sánchez, M. Utili, F.G. Ferré, F.D. Fonzo, Efficient hydrogen and deuterium permeation reduction in Al2O3 coatings with enhanced radiation tolerance and corrosion resistance, Nucl. Fusion 58 (2018) 126007, https://doi.org/10.1088/1741-4326/aadd1d.

[7] M. Utili, S. Bassini, S. Cataldo, F. Di Fonzo, M. Kordac, T. Hernandez, K. Kunzova, J. Lorenz, D. Martelli, B. Padino, A. Moroño, M. Tarantino, C. Schroer, G. A. Spagnuolo, L. Vala, M. Vanazzi, A. Venturini, Development of anti-permeation and corrosion barrier coatings for the WCLL breeding blanket of the European DEMO, Fusion Eng. Des. 170 (2021) 112453, https://doi.org/10.1016/j.fusengdes.2021.112453.

[8] R. González-Arrabal, E. Carella, F.J. Sánchez, G. de la Cuerda-Velázquez, G. García, J.M. Perlado, T. Hernández, Characterization of the lithium concentration and distribution as a function of depth for alumina coatings after exposure to PbLi, J. Nucl. Mater. (2023) 154688, https://doi.org/10.1016/j.jnucmat.2023.154688.

[9] E. Carella, G. de la Cuerda-Velázquez, M. Angiolini, R. González-Arrabal, A. Bulla, I. Palermo, F. Di Fonzo, F. Sanchez, A.J. London, T. Hernández, A. Moroño, A. Stinchelli, M. Moody, G.A. Spagnuolo, Exploring the role of lithium in Al2O3 tritium permeation barrier development: a crucial challenge for fusion reactor progress, J. Nucl. Mater. 602 (2024) 155354, https://doi.org/10.1016/j.jnucmat.2024.155354.

[10] I. Palermo, J. Mauricio Garcia, M. González, M. Malo, D. Rapisarda, Radiological characterization of ceramic materials considered for the HT-DCLL DEMO reactor, Nuclear Materials and Energy 30 (2022) 101136, https://doi.org/10.1016/j.nme.2022.101136.

[11] G.L. Harris, Properties of Silicon Carbide, IEE, INSPEC, London, U.K., 1995.

[12] T. Chikada, A. Suzuki, T. Terai, Deuterium permeation and thermal behaviors of amorphous silicon carbide coatings on steels, Fusion Engineering and Design 86 (2011) 2192–2195, https://doi.org/10.1016/j.fusengdes.2011.01.036.

[13] Z. Yao, A. Suzuki, D. Levchuk, T. Terai, SiC coating by RF sputtering as tritium permeation barrier for fusion blanket, Fusion Sci. Technol. 52 (2007) 865–869, https://doi.org/10.13182/FST07-A1601.

[14] T. Hernández, A. Moroño, F.J. Sánchez, C. Maffiotte, M.A. Monclús, R. González-Arrabal, Study of deuterium permeation, retention, and desorption in SiC coatings submitted to relevant conditions for breeder blanket applications: thermal cycling effect under electron irradiation and oxygen exposure, J. Nucl. Mater. 557 (2021) 153219, https://doi.org/10.1016/j.jnucmat.2021.153219.

[15] K.-I. Park, J.-H. Kim, H.-K. Lee, D.K. Kim, High temperature mechanical properties of CVD-SiC thin films, Mod. Phys. Lett. B 23 (2009) 3877–3886, https://doi.org/10.1142/S0217984909021946.

[16] A.E. Kaloyeros, B. Arkles, Silicon carbide thin film technologies: recent advances in processing, properties, and applications - part I thermal and plasma CVD, ECS J. Solid State Sci. Technol. 12 (2023) 103001, https://doi.org/10.1149/2162-8777/acf8f5.

[17] M. Oujja, K. Tabakkouht, M. Sanz, E. Rebollar, M. Sánchez-Arenillas, J.F. Marco, M. Castillejo, R. de Nalda, Synthesis of smooth amorphous thin films of silicon carbide with controlled properties through pulsed laser deposition, Appl. Phys. A Mater. Sci. Process. 128 (2022) 375, https://doi.org/10.1007/s00339-022-05499-9.

[18] D. Hagedorn, F. Löffler, R. Meeß, Magnetron sputter process for inner cylinder coatings, Surf. Coat. Technol. 203 (2008) 632–637, https://doi.org/10.1016/j.surfcoat.2008.06.166.

[19] Nano4Energy.eu, Nano4Energy (n.d.). https://nano4energy.eu/ (accessed January 19, 2024).

[20] Z. Zhong, T. Hinoki, A. Kohyama, Microstructure and mechanical strength of diffusion bonded joints between silicon carbide and F82H steel, J. Nucl. Mater. 417 (2011) 395–399, https://doi.org/10.1016/j.jnucmat.2010.12.252.

[21] A. Redondo-Cubero, M.J.G. Borge, N. Gordillo, P.C. Gutiérrez, J. Olivares, R. Pérez Casero, M.D. Ynsa, Current status and future developments of the ion beam facility at the Centre of micro-analysis of materials in Madrid, Eur. Phys. J. Plus 136 (2021) 175, https://doi.org/10.1140/epjp/s13360-021-01085-9.

[22] J.A. Leavitt, L.C. McIntyre, P. Stoss, J.G. Oder, M.D. Ashbaugh, B. Dezfouly-Arjomandy, Z.M. Yang, Z. Lin, Cross sections for 170.5 ° backscattering of 4He from carbon for 4He energies between 1.6 and 5.0 MeV, Nucl. Instrum. Methods Phys. Res., Sect. B 40–41 (1989) 776–779, https://doi.org/10.1016/0168-583X(89)90476-X.

[23] H. Cheng, H. Shen, F. Yang, J. Tang, Cross sections for non-Rutherford backscattering of 4He from five light elements, Nucl. Instrum. Methods Phys. Res., Sect. B 85 (1994) 47–50, https://doi.org/10.1016/0168-583X(94)95783-5.

[24] W.C. Oliver, G.M. Pharr, An improved technique for determining hardness and elastic modulus using load and displacement sensing indentation experiments, J. Mater. Res. 7 (1992) 1564–1583, https://doi.org/10.1557/JMR.1992.1564.

[25] J. Tomastik, R. Ctvrtlik, Nanoscratch test — a tool for evaluation of cohesive and adhesive properties of thin films and coatings, EPJ Web of Conferences 48 (2013) 00027, https://doi.org/10.1051/epjconf/20134800027.

[26] J.A. Thornton, Influence of apparatus geometry and deposition conditions on the structure and topography of thick sputtered coatings, journal of vacuum, Sci. Technol. 11 (1974) 666–670, https://doi.org/10.1116/1.1312732.

[27] J.A. Thornton, Influence of substrate temperature and deposition rate on structure of thick sputtered cu coatings, journal of vacuum, For. Sci. Technol. 12 (1975) 830–835, https://doi.org/10.1116/1.568682.

[28] Y. Wu, S. Zhu, Y. Zhang, T. Liu, Y. Rao, lizhu Luo, Q, Wang, The adhesion strength and deuterium permeation property of SiC films synthesized by magnetron sputtering, International Journal of Hydrogen Energy 41 (2016) 10827–10832, https://doi.org/10.1016/j.ijhydene.2016.04.233.

[29] H. Tang, S. Tan, Z. Huang, S. Dong, D. Jiang, Surface morphology of α-SIC coatings deposited by RF magnetron sputtering, Surf. Coat. Technol. 197 (2005) 161–167, https://doi.org/10.1016/j.surfcoat.2004.11.036.

[30] O.P. Oladijo, M.R. Sanjay, L.L. Collieus, S. Siengchin, L. Moloisane, S.S. Oladijo, Effects of deposition time and RF power on the film characteristics of magnetron sputtered silicon carbide thin films, Materials Today: Proceedings 52 (2022) 2432–2438, https://doi.org/10.1016/j.matpr.2021.10.423.

[31] M. Liu, Y. Yang, Q. Mao, Y. Wei, Y. Li, N. Ma, H. Liu, X. Liu, Z. Huang, Influence of radio frequency magnetron sputtering parameters on the structure and performance of SiC films, Ceram. Int. 47 (2021) 24098–24105, https://doi.org/10.1016/j.ceramint.2021.05.120.

[32] T. Takagi, Ion–surface interactions during thin film deposition, J. Vac. Sci. Technol. A 2 (1984) 382–388, https://doi.org/10.1116/1.572748.

[33] Y.-L. Kuo, J.-J. Huang, S.-T. Lin, C. Lee, W.-H. Lee, Diffusion barrier properties of sputtered TaNx between cu and Si using TaN as the target, Mater. Chem. Phys. 80 (2003) 690–695, https://doi.org/10.1016/S0254-0584(03)00106-8.

[34] K.-S. Kim, K.-A. Lee, Room temperature impact-induced deposition of pure SiC coating layer by vacuum kinetic spraying, J. Am. Ceram. Soc. 103 (2020) 54–59, https://doi.org/10.1111/jace.16688.

[35] M. Mayer, SIMNRA User's Guide, Report IPP 9–113 Max-Planck-Institut für Plasmaphysik, Garching, Germany, 1997.

[36] A.K. Costa, S.S. Camargo, C.A. Achete, R. Carius, Characterization of ultra-hard silicon carbide coatings deposited by RF magnetron sputtering, Thin Solid Films 377–378 (2000) 243–248, https://doi.org/10.1016/S0040-6090(00)01321-3.

[37] S. Gangopadhyay, R. Acharya, A.K. Chattopadhyay, S. Paul, Effect of substrate bias voltage on structural and mechanical properties of pulsed DC magnetron sputtered TiN–MoSx composite coatings, Vacuum 84 (2010) 843–850, https://doi.org/10.1016/j.vacuum.2009.11.010.

[38] D. Bhaduri, A. Ghosh, S. Gangopadhyay, S. Paul, Effect of target frequency, bias voltage and bias frequency on microstructure and mechanical properties of pulsed DC CFUBM sputtered TiN coating, Surf. Coat. Technol. 204 (2010) 3684–3697, https://doi.org/10.1016/j.surfcoat.2010.04.047.

[39] Q. Ma, L. Li, Y. Xu, J. Gu, L. Wang, Y. Xu, Effect of bias voltage on TiAlSiN nanocomposite coatings deposited by HiPIMS, Appl. Surf. Sci. 392 (2017) 826–833, https://doi.org/10.1016/j.apsusc.2016.09.028.

[40] D.M. Devia, E. Restrepo-Parra, P.J. Arango, A.P. Tschiptschin, J.M. Velez, TiAlN coatings deposited by triode magnetron sputtering varying the bias voltage, Appl. Surf. Sci. 257 (2011) 6181–6185, https://doi.org/10.1016/j.apsusc.2011.02.027.

[41] M. Naka, J.C. Feng, J.C. Schuster, Phase reactions and diffusion path of the SiC/Cr system, J. Mater. Synth. Process. 6 (1998) 169–173, https://doi.org/10.1023/A:1022617502576.

[42] M. Naka, J.C. Feng, J.C. Schuster, Phase reaction and diffusion path of the SiC/Ti system, Metall. Mater. Trans. A 28 (1997) 1385–1390, https://doi.org/10.1007/s11661-997-0275-3.

[43] L. Li, W. Jin, H. Yang, K. Gao, P. Guo, X. Pang, A.A. Volinsky, First principles calculations study of crystallographic orientation effects on SiC/Ti and SiC/Cr interfaces, Microelectron. Reliab. 83 (2018) 119–126, https://doi.org/10.1016/j.microrel.2018.02.019.